J. Fluid Mech. (2005), *vol.* 528, *pp.* 233–254. © 2005 Cambridge University Press
doi:10.1017/S0022112004003295 Printed in the United Kingdom

Lattice-Boltzmann simulations of low-Reynolds-number flow past mono- and bidisperse arrays of spheres: results for the permeability and drag force

By M. A. VAN DER HOEF, R. BEETSTRA AND J. A. M. KUIPERS

Department of Science and Technology, University of Twente, PO Box 217, 7500 AE Enschede, The Netherlands

(Received 24 March 2004 and in revised form 18 November 2004)

We report on lattice-Boltzmann simulations of slow fluid flow past mono- and bidisperse random arrays of spheres. We have measured the drag force on the spheres for a range of diameter ratios, mass fractions and packing fractions; in total, we studied 58 different parameter sets. Our simulation data for the permeability agrees well with previous simulation results and the experimental findings. On the basis of our data for the individual drag force, we have formulated new drag force relations for both monodisperse and polydisperse systems, based on the Carman–Kozeny equations; the average deviation of our binary simulation data with the new relation is less than 5%. We expect that these new relations will significantly improve the numerical modelling of gas–solid systems with polydisperse particles, in particular with respect to mixing and segregation phenomena. For binary systems with large diameter ratios (1:4), the individual drag force on a particle, as calculated from our relations, can differ by up to a factor of five compared with predictions presently favoured in chemical engineering.

1. Introduction

Understanding, and hence predicting, the resistance behaviour of densely packed solid particles to fluid flow has proved to be difficult. Even for the most simple model systems (static, random arrays of monodisperse spheres) there is no definitive consensus regarding the precise form of the drag force on the spheres (e.g. see figure 1); little, if anything, is known about the drag force for systems which deviate from the model conditions. Accurate drag force relations are, however, of great practical importance. In particular, in chemical engineering, drag force relations are widely used in the numerical models that predict the flow behaviour of gas and liquid fluidized beds of granular material (van Swaaij 1985; Gidaspow 1994; Hoomans *et al.* 1996; Kuipers & van Swaaij 1998). Such beds form an essential part of many industrially important chemical reactors, of which the fluid catalytic cracking (FCC) reactor is a prototypical example. In previous studies, it was found that the flow behaviour of gas fluidized beds can be very sensitive to the precise functional form of the drag force, in particular how it varies with the gas fraction (Li & Kuipers 2003). To date, mainly empirical relations have been used, such as the Ergun (1952) and Wen & Yu (1966) equations for monodisperse systems. Only recently, new drag force relations were proposed by Koch and coworkers (Koch & Sangani 1999; Koch &

https://doi.org/10.1017/S0022112004003295 Published online by Cambridge University Press

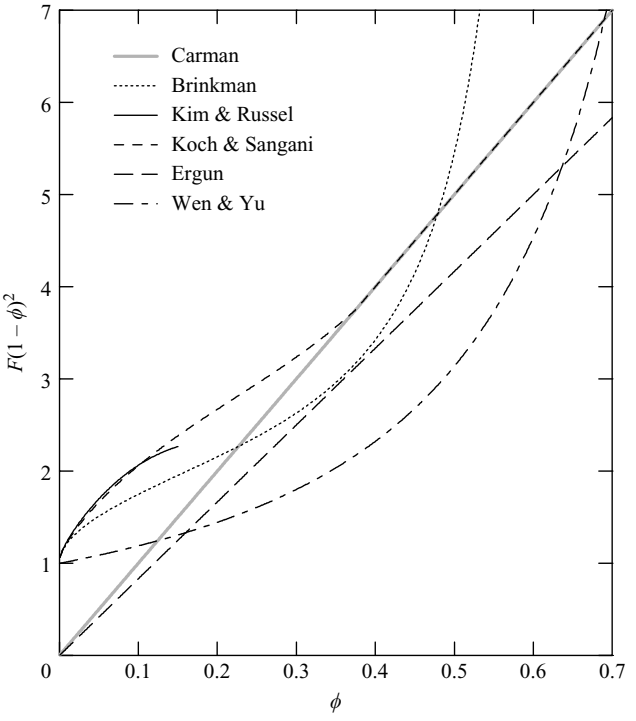

FIGURE 1. Normalized drag force (multiplied by the porosity squared) as a function of the packing fraction ϕ; the figure shows some well-known drag force relations, obtained from experiment, theory and simulation.

Hill 2001; Hill, Koch & Ladd 2001*a*, *b*), based on accurate numerical data from lattice-Boltzmann simulations. In these simulations, the flow field around the spheres is calculated from a discretized version of the Boltzmann equation, with a grid that is 10–30 times smaller than the diameter of the spheres. A recent discrete particle study by Bokkers, van Sint Annaland & Kuipers (2004) showed that, with respect to bubble formation in fluidized beds, the drag relations derived from the lattice-Boltzmann simulations yielded better agreement with the experimental observations than the traditional Ergun and Wen & Yu correlations. Although these latter relations remain the most widely used to date in chemical engineering, a consensus is growing that relations such as those proposed by Koch and coworkers, do provide the most accurate description for the interphase momentum transfer, at least for ideal systems, that is, for monodisperse, homogeneous and static systems; in practical applications, however, such ideal conditions are hardly ever encountered. In this paper, a first step is made towards describing the drag force for non-ideal systems, where we want to investigate the effect of polydispersity. We focus our studies on binary systems, although the drag force relation that we propose here is derived for general polydisperse systems. Koo & Sangani (2002) applied the effective medium theory to binary systems, and found that the predictions for the individual drag force were in good agreement with the results from multipole expansions methods. The theory was also found to predict well the average hydrodynamic properties and conditionally averaged velocity fields. The drawback of the effective medium theory, however, is that it requires the cumbersome task of evaluating structure factors in the bidisperse suspensions. In that respect, the lattice-Boltzmann simulations provide a more simple and direct way

https://doi.org/10.1017/S0022112004003295 Published online by Cambridge University Press

of arriving at accurate results for the drag force, especially since binary systems are not more difficult to simulate than monodisperse systems. In the simulations, we consider only systems where the configuration of the particles is static. The effect of the granular temperature on the drag force will be addressed in future publications.

The simulation method that we use is very similar to the method employed by Hill *et al.* (2001*a*, *b*) to measure the drag force in monodisperse systems. In fact, we use the same lattice-Boltzmann suspension code SUSP3D, developed by Ladd. We have also performed extensive simulations on monodisperse systems because: (i) We want to present the drag force for bidisperse systems in terms of a deviation from the monodisperse drag force. Since these deviations can be rather small, we decided to perform a new set of accurate simulations on monodisperse systems; on average, the error margin on our data is a factor of two smaller compared to the data of Hill *et al.* (2001*a*, *b*); we use this new data to formulate a new and more accurate drag force correlation for monodisperse systems. (ii) A direct comparison of our binary data with the monodisperse data of Hill *et al.* (2001*a*, *b*) could introduce some systematic errors, since we measure the drag force in a different way, as will be discussed in § 3.3. (iii) Since we have rather large diameter ratios (up to 4:1), we are forced to use relatively small particles in the simulations, in order to keep the computer time within reasonable limits. For this reason, we also study the effect of particle size, relative to the gridsize, on the drag force in monodisperse systems.

In the next section, we give a brief overview of drag force relations for monodisperse and bidisperse system, in which we also suggest a new drag force relation for bidisperse systems. This is followed by a more elaborate discussion of the simulation method; in § 4, we present our simulation results for both monodisperse and bidisperse systems, and in the last section we summarize the most important results and present some concluding remarks.

2. Overview of drag force relations

2.1. *Definitions*

We start by noting that there exists some ambiguity in the literature on the precise definition of the drag force, in particular, as to whether the contribution of the pressure gradient should be included. In order to avoid any confusion, and also to define the notation for the remainder of the paper, we briefly describe the relation of the drag force to the pressure drop. To this end, we consider a model system with a total volume V_{tot}, which contains N monodisperse spheres (diameter d, volume V), randomly distributed over space, and fixed to their positions. An incompressible continuum phase, characterized by a mass density ρ and shear viscosity μ, is flowing through the bed at constant velocity $\boldsymbol{u}$. In the remainder of the paper, we will denote this continuum phase as gas, but the results are equally valid for particles suspended in a liquid. The solid volume fraction ϕ and particle Reynolds number Re are defined by

$$\phi = \frac{NV}{V_{tot}}, \qquad Re = \frac{\rho|U|d}{\mu}, \qquad \boldsymbol{U} = (1-\phi)\boldsymbol{u}, \tag{1}$$

where $\boldsymbol{U}$ is the superficial gas velocity, defined as the gas velocity averaged over the total volume of the system. Since the gas is flowing with constant velocity, the total force on the gas should be zero, and thus:

$$-V_{tot}\boldsymbol{\nabla} P - N\boldsymbol{F}_{g\rightarrow s} = 0, \tag{2}$$

https://doi.org/10.1017/S0022112004003295 Published online by Cambridge University Press

with ∇P the pressure gradient across the volume, and $\boldsymbol{F}_{g\rightarrow s}$ the total average force that the gas exerts on each particle. There are two contributions to this force, namely,

$$\boldsymbol{F}_{g\rightarrow s} = \boldsymbol{F}_d - V\boldsymbol{\nabla} P. \tag{3}$$

The first term is the drag force $\boldsymbol{F}_d$, which results from the friction between the particle and the gas at the surface of the particle, which is present whenever the difference between gas- and particle-velocity is non-zero. The second term is the buoyancy-type force due to the pressure gradient. Combining (2) and (3) gives:

$$\boldsymbol{F}_d = -\frac{1-\phi}{\phi} V\boldsymbol{\nabla} P. \tag{4}$$

Note that in some literature (e.g. Hill *et al.* 2001*a*, *b*), the total force on the particle $\boldsymbol{F}_{g\rightarrow s}$ is defined as the drag force. From the analysis above, it follows that

$$\boldsymbol{F}_{g\rightarrow s} = \boldsymbol{F}_d/(1-\phi), \tag{5}$$

i.e. two definitions differ by a factor $(1-\phi)$. In this paper, we define $\boldsymbol{F}_d$ as the drag force, which is a common choice in chemical engineering (e.g. see Di Felice 1995); this is because in the numerical models it is more natural to couple the force due to the pressure gradient with the gravity-induced buoyancy force, rather than with the drag force.

In the limit of infinite dilution, and when inertial effects can be neglected, the drag force takes the Stokes–Einstein form $\boldsymbol{F}_d = 3\pi\mu d\boldsymbol{U}$. It is therefore convenient to define the dimensionless drag force

$$F = \frac{\boldsymbol{F}_d}{3\pi\mu d\boldsymbol{U}}, \tag{6}$$

such that $F \rightarrow 1$ in the limit $\phi \rightarrow 0$, $Re \rightarrow 0$. We will use this representation of the drag force in the remainder of the paper. It then follows that

$$\frac{(1-\phi)}{\phi}\boldsymbol{\nabla} P = -18\mu\boldsymbol{U}\frac{F}{d^2}. \tag{7}$$

Note that in chemical engineering, the drag force is traditionally described via a friction coefficient β (e.g. see Gidaspow 1994). The relation between β and F is

$$\beta = 18\mu(1-\phi)\phi\frac{F}{d^2}.$$

2.2. *Drag force relations for monodisperse systems*

A useful starting point for describing Stokes flow through a dense random array of spheres is the Darcy equation:

$$\boldsymbol{\nabla} P = -\frac{1}{\kappa}\mu\boldsymbol{U}, \tag{8}$$

which is a general relation for the pressure drop over a porous medium. In (8), κ is defined as the permeability of the medium, which depends – in principle – on the geometrical details of the system. In practice, however, the permeability is found to be described well by the Carman–Kozeny approximation:

$$\kappa = (1-\phi)\frac{r_h^2}{k}, \tag{9}$$

where k is the Kozeny constant, whose value is usually found to be close to 5 (independent of the geometry), and r_h is the hydraulic radius, defined as the ratio of

https://doi.org/10.1017/S0022112004003295 Published online by Cambridge University Press

the free volume to the 'wetted area'. The basic idea behind this assumption is that the medium can be considered as a system of channels of width r_h; equation (9) then follows from assuming a Poiseuille-type law for the pressure drop over the channels. For monodisperse spheres,

$$r_h = \frac{1-\phi}{6\phi}\, d, \tag{10}$$

which combined with (7) to (10) gives the Carman–Kozeny (CK) relation for the drag force:

$$F = 2k\frac{\phi}{(1-\phi)^2}. \tag{11}$$

For $k=5$, equation (11) is known as the Carman equation, for $k=4.167$, equation (11) represents the $Re=0$ limit of the Ergun equation (also known as the Blake–Carman–Kozeny equation). One of the limitations of the CK relation is that it is only valid for dense arrays, which is underlined by the fact that it does not have the correct limit $F\to 1$ for $\phi\to 0$. For that limit, Kim & Russel (1985) derived the following expression for F:

$$F = (1-\phi)\left[1+\frac{3}{\sqrt{2}}\sqrt{\phi}+\frac{135}{64}\phi\ln\phi+16.456\phi+\cdots\right], \tag{12}$$

which was found to be in perfect agreement with the computer simulations by Ladd (1990) and Hill *et al.* (2001*a*, *b*). Several attempts have been made to find expressions for F valid over the entire solid fraction range. One of the earliest, obtained from theory, is the well-known Brinkman equation:

$$F = (1-\phi)\left(1+\tfrac{3}{4}\phi\left[1-\sqrt{\frac{8}{\phi}-3}\right]\right)^{-1}. \tag{13}$$

In the limit $\phi\to 0$, equation (13) is to lowest order in ϕ equivalent to (12). In the range $0.20<\phi<0.50$, the Brinkman equation predicts a drag force that is slightly lower than the Carman equation, whereas for $\phi>0.50$, the Brinkman equation seriously overpredicts the drag force, since it diverges at $\phi=2/3$. Koch & Sangani (1999) proposed the following expression for the drag force:

$$F = \begin{cases} \dfrac{(1-\phi)\left(1+\frac{3}{\sqrt{2}}\phi^{1/2}+\frac{135}{64}\phi\ln\phi+16.14\phi\right)}{1+0.681\phi-8.48\phi^2+8.16\phi^3} & \text{for}\quad \phi<0.4, \\ 10\dfrac{\phi}{(1-\phi)^2} & \text{for}\quad \phi>0.4, \end{cases} \tag{14}$$

that is, for large volume fraction, F is given by the Carman relation, (11), whereas for ϕ close to zero, F is equal to (12) to order ϕ. Equation (14) was found to be in good agreement with the results from lattice-Boltzmann simulations. Finally, in chemical engineering models of gas fluidized beds, the combination of the Ergun and Wen & Yu equation have found widespread use:

$$F = \begin{cases} (1-\phi)^{-3.65}(1+0.15Re^{0.687}) & (\phi<0.2), \\ \dfrac{150}{18}\dfrac{\phi}{(1-\phi)^2}+\dfrac{1.75}{18}\dfrac{Re}{(1-\phi)^2} & (\phi>0.2). \end{cases} \tag{15}$$

As mentioned before, in the limit $Re\to 0$, the Ergun equation is equal to the CK relation, (11), with $k=150/36=4.167$. The Ergun equation is based on experimental

https://doi.org/10.1017/S0022112004003295 Published online by Cambridge University Press

data for the pressure drop over fixed dense beds of spheres, whereas the Wen & Yu equation is based on data for the terminal velocity of sedimenting spheres at different porosities. In figure 1 we compare the various drag force relations that we have listed in this section. It is clear that there are significant deviations between the various predictions from theory, experiment and simulation.

2.3. *Drag force relations for polydisperse systems*

We next consider a polydisperse system, which contains N_i spheres of type i (diameter d_i, volume V_i), with $i = 1, 2, \ldots, c$. We define the normalized drag force F_i, the mass fraction x_i and the diameter fraction y_i as

$$F_i = \frac{\boldsymbol{F}_{d,i}}{3\pi\mu d_i \boldsymbol{U}}, \qquad x_i = \frac{\phi_i}{\phi}, \qquad y_i = \frac{d_i}{\langle d \rangle}, \tag{16}$$

with $\boldsymbol{F}_{d,i}$ the drag force on a particle of type i, $\phi_i = N_i V_i / V_{tot}$ the partial volume fraction, and $\langle d \rangle$ the average diameter defined as

$$\langle d \rangle = \frac{\sum_{i=1}^{c} N_i d_i^3}{\sum_{i=1}^{c} N_i d_i^2} = \left[\sum_{i=1}^{c} \frac{x_i}{d_i} \right]^{-1}. \tag{17}$$

The relation between the pressure gradient and the drag force, as derived in § 2.1, can be readily extended to polydisperse systems, and is equal to

$$\frac{(1-\phi)}{\phi} \boldsymbol{\nabla} P = -18\mu \boldsymbol{U} \left[\sum_{i=1}^{c} \frac{x_i}{d_i^2} F_i \right] = -18\mu \boldsymbol{U} \frac{\langle F \rangle}{\langle d \rangle^2}, \tag{18}$$

where, in the last step, we have cast it in the same form as the monodisperse relation (7), with d replaced by $\langle d \rangle$, and F replaced by a weighted average drag force defined by

$$\langle F \rangle = \sum_{i=1}^{c} \frac{x_i}{y_i^2} F_i. \tag{19}$$

We next generalize the CK relations to polydisperse systems. It can easily be shown that the hydraulic radius for such systems has the same form as (10), only with d replaced by the average diameter $\langle d \rangle$. As a result, combining (8)–(10) with (18) gives

$$\langle F \rangle = 2k \frac{\phi}{(1-\phi)^2}. \tag{20}$$

Comparison with (11) shows that the average drag force for polydisperse systems, as defined by (19), is equal to the monodisperse drag force, at least in the Carman–Kozeny approximation:

$$\langle F \rangle = F(\phi), \tag{21}$$

This approach, however, yields only an expression for the average drag force $\langle F \rangle$, and not for the individual force F_i on each type of particle. Although polydisperse systems are frequently encountered in gas fluidized beds, at present rather *ad hoc* modifications of the monodisperse relations are employed (Gidaspow 1994), where d is simply replaced by d_i; that is, for low Reynolds numbers, the normalized drag force F_i of the individual species is assumed to be equal to the normalized drag force F of a monodisperse system at the same volume fraction. It can immediately be seen from the definition (19), however, that $F_i = F$ does not satisfy (21); to our knowledge,

https://doi.org/10.1017/S0022112004003295 Published online by Cambridge University Press

only one attempt has been made in literature to formulate an improved expression for the individual drag force.

In the model by Patwardhan & Tien (1985), the individual drag force F_i is also taken to be equal to the monodisperse drag force, but now at a volume fraction $\phi^{(i)}$, instead of the overall volume fraction ϕ, namely,

$$F_i(\phi) = F\left(\phi^{(i)}\right).$$

The underlying idea is that the effective porosity which a particle experiences is primarily dominated by the distance to its neighbouring particles; for instance, if the distance is larger, the flow profile is less disturbed, and thus the effective porosity that the particle experiences is larger (thus $\phi^{(i)} < \phi$). This distance is estimated by δ, which is defined such that the volume of spheres with diameter $d_i + \delta$ is equal to the total volume, namely,

$$\sum_{i=1}^{c} N_i \tfrac{1}{6}\pi(d_i + \delta)^3 = V_{tot}. \tag{22}$$

The effective packing fraction $\phi^{(i)}$ of particles of type i is then estimated as the packing fraction that a monodisperse system with $d = d_i$ would have with the same δ, which is given by

$$\frac{1}{\phi^{(i)}} = \left(1 + \frac{\delta}{d_i}\right)^3. \tag{23}$$

The main difficulty of this approach lies in evaluating δ from (22). For monodisperse systems, δ can be readily evaluated: $\delta = d[\phi^{-1/3} - 1]$. Patwardhan & Tien approximate the solution for polydisperse systems by

$$\delta = d_{avg}\left[\phi^{-1/3} - 1\right], \qquad d_{avg} = \sum_i x_i d_i. \tag{24}$$

However, this choice for d_{avg} seems to be *ad hoc*, and no justification is given. As we will show in § 5, a significant improvement is achieved by using $d_{avg} = \langle d \rangle$. In fact, it is possible to obtain the exact solution for δ – at least numerically – since (22) can be cast in the form

$$\frac{1}{\phi} = 1 + 3\frac{\delta}{\langle d \rangle} + 3\frac{\delta^2}{\langle d^2 \rangle} + \frac{\delta^3}{\langle d^3 \rangle}, \tag{25}$$

with $\langle d \rangle$ given by (17), and $\langle d^2 \rangle$, $\langle d^3 \rangle$ defined in a similar fashion:

$$\langle d^2 \rangle = \frac{\sum_{i=1}^{c} N_i d_i^3}{\sum_{i=1}^{c} N_i d_i} = \left[\sum_{i=1}^{c} \frac{x_i}{d_i^2}\right]^{-1}, \qquad \langle d^3 \rangle = \frac{\sum_{i=1}^{c} N_i d_i^3}{\sum_{i=1}^{c} N_i} = \left[\sum_{i=1}^{c} \frac{x_i}{d_i^3}\right]^{-1}.$$

Note that if $\langle d^n \rangle = \langle d \rangle^n$, the solution of (25) would indeed be given by (24), with $d_{avg} = \langle d \rangle$. In § 4, we will compare the predictions of the Patwardhan & Tien model, using different estimates for δ, with our simulation results. One of the drawbacks of this approach is that it does not yield an explicit expression for F_i in terms of the parameters x_i and y_i. In the next section, we will derive such an explicit expression.

2.4. *A new drag force relation for polydisperse systems*

One of the shortcomings of both the approximate expressions $F_i(\phi) = F(\phi)$ and $F_i(\phi) = F(\phi^{(i)})$ is that these do not satisfy the basic relation (21). It is possible, however, to formulate two relations which do satisfy (21), namely $F_i(\phi) = y_i F(\phi)$

https://doi.org/10.1017/S0022112004003295 Published online by Cambridge University Press

and $F_i = y_i^2 F(\phi)$. The first solution would imply that $F_i/F_j = d_i/d_j$, whereas the second solution gives $F_i/F_j = (d_i/d_j)^2$. Our lattice-Boltzmann simulations (which we will discuss later in this paper) show that, for binary systems, $F_i/F_j = (d_i/d_j)^n$ with $1 < n < 2$ (see figure 7), which suggests that we should try a general solution as a linear combination:

$$F_i = \left((1-f)y_i + f y_i^2\right) F \qquad (0 \leqslant f \leqslant 1). \tag{26}$$

The unknown factor f may be determined from the limit $d_i/d_j \to 0$, $\forall\, j \neq i$, while ϕ_i and ϕ are kept constant. In that limit, $y_i = x_i$, and therefore (26) reduces to

$$\lim_{d_i/d_j \to 0} F_i = x_i\,(1 - f + f x_i)\, F. \tag{27}$$

On the other hand, for this limit, we may consider a system where d_i is kept constant, while all the other spheres of type $j \neq i$ grow infinitely large. From the point of view of the type i spheres, this system is then effectively monodisperse, with the available volume reduced by $\sum_{j \neq i} N_j V_j$. Thus, in that limit, F_i is equal to the monodisperse drag force at a modified packing fraction ϕ':

$$\lim_{d_i/d_j \to 0} F_i = 2k\frac{\phi'}{(1-\phi')^2}, \qquad \phi' = \frac{N_i V_i}{V - \sum_{j \neq i} N_j V_j} = \frac{\phi_i}{1 - \phi + \phi_i}.$$

Using (11), we obtain

$$\lim_{d_i/d_j \to 0} F_i = x_i\,(1 - \phi + \phi x_i)\, F.$$

Comparing with (27) gives $f = \phi$. Note that from these expressions, it follows that the permeability of the polydisperse system is given by

$$\kappa = \langle d \rangle^2 \frac{1-\phi}{18\phi F} = \langle d \rangle^2 \frac{(1-\phi)^3}{36\,k\phi^2}.$$

For binary systems, the limit $d_1/d_2 \to \infty$ gives $\langle d \rangle = d_2/x_2$, and thus

$$\lim_{d_1/d_2 \to \infty} \kappa = d_2^2 \frac{(1-\phi)^3}{36\,k\phi_2^2},$$

which is in agreement with the exact result from Sangani & Yao (1988) in the same limit (see also § 2 of Thies-Weesie & Philipse 1994).

Up to this point, all derivations have been made within the framework of the Carman–Kozeny approximation, which is valid for dense packings only. The final assumption we now make is that the relation between F_i and F (and thus also between $\langle F \rangle$ and F) is generally valid, i.e. that for the monodisperse drag force F in (21) and (26), we can use the best possible fit (31), valid over the entire packing fraction range. In § 4, we will test the validity of (26) using this assumption, by comparing with the results from lattice-Boltzmann simulations. In the next section, we will discuss this simulation method in detail.

3. Simulation method

The momentum exchange between the solid and the gas phase is completely determined by the interaction of the gas phase with the surface of the solid phase; for instance, the Stokes drag force $F_d = 3\pi\mu d u$ on an isolated sphere follows from the equations of hydrodynamics with 'stick boundary' conditions for the gas at the solid surface. Therefore, it is essential that the numerical method describes the flow

https://doi.org/10.1017/S0022112004003295 Published online by Cambridge University Press

field at scales of at least one order smaller than the diameter of the spheres, so that their surface can be adequately resolved. In this work, the lattice-Boltzmann method is used to solve the equations of hydrodynamics, with stick boundary rules applied at the surface of the solid phase. In the next section, we will briefly go over the essential features of the method, followed by a more elaborate discussion of the measurement procedure and the finite size effects.

3.1. *Lattice-Boltzmann model*

A general overview of lattice-Boltzmann methods can be found in Chen & Doolen (1998) and Succi (2001), amongst others. An elaborate description of the specific method that we have used, including the modelling of the solid–gas boundary, can be found in the overview papers by Ladd (1993*a*, *b*) and Ladd & Verberg (2001). Here, we will discuss the method only briefly in general terms. The lattice-Boltzmann model is basically a finite-difference scheme for solving the Boltzmann equation. In its most simple form, the finite-difference scheme reads:

$$f(\boldsymbol{v}, \boldsymbol{r} + \boldsymbol{v}\delta t, t + \delta t) - f(\boldsymbol{v}, \boldsymbol{r}, t) = -\frac{\delta t}{\tau}\left(f(\boldsymbol{v}, \boldsymbol{r}, t) - f^{eq}(\boldsymbol{v}, \boldsymbol{r}, t)\right) \tag{28}$$

where f is the single particle distribution function, which is equivalent to the gas density in the six-dimensional velocity-coordinate space, and f^{eq} represents the equilibrium distribution. In (28), the position $\boldsymbol{r}$ and velocity $\boldsymbol{v}$ are discrete, i.e. the possible positions are restricted to the sites of a lattice, and thus the possible velocities are vectors connecting nearest neighbour sites of this lattice. Note that (28) represents a propagation, followed by a relaxation to the equilibrium distribution, which is the ensemble average effect of gas particle collisions. From the single-particle distribution function, the hydrodynamic variables of interest – the local gas density ρ and velocity $\boldsymbol{u}$ – are obtained by taking the zeroth and first moment:

$$\rho(\boldsymbol{r}, t) = \sum_{v} f(\boldsymbol{v}, \boldsymbol{r}, t), \qquad \rho(\boldsymbol{r}, t)\boldsymbol{u}(\boldsymbol{r}, t) = \sum_{v} \boldsymbol{v} f(\boldsymbol{v}, \boldsymbol{r}, t). \tag{29}$$

The zeroth moment of (28) directly yields the conservation of mass equation. The first moment of (28) will give an equation that is to order δt^2 equivalent to the Navier–Stokes equation of an incompressible gas, with a viscosity given in terms of the relaxation time τ. One of the advantages of the LB model over other finite-difference models for gas flow, is that boundary conditions can be modelled in a very simple way. In particular, non-static boundaries, even with an irregular shape, are not more costly to simulate than straight static boundaries. A particularly efficient and simple way to enforce stick boundary rules was introduced by Ladd (1993*a*, *b*). First, the boundary nodes are identified. They are defined as the points halfway between any pair of neighbouring lattice sites, of which one is located inside the sphere, and the other one outside the sphere. For a static particle, the boundary rule is simply that a distribution moving such that it would cross the boundary, bounces back at the boundary node; from (29), it then follows that this will result in a zero average velocity at the boundary node. For moving and rotating particles, the rules involve some simple modifications of the bounce back rule, depending on the local boundary velocity. For details we refer to Ladd (1993*a*, *b*) and Ladd & Verberg (2001). The total change in gas momentum due to the boundary rule at all the boundary nodes on a single sphere is then equal to the $-\boldsymbol{F}_{g\to s}$, with $\boldsymbol{F}_{g\to s}$ the total force that the gas exerts on the sphere, from which the drag force $\boldsymbol{F}_d$ can be obtained directly (see § 2.1).

https://doi.org/10.1017/S0022112004003295 Published online by Cambridge University Press

3.2. *Simulation set-up*

For a description of the simulation set-up, we restrict ourselves to monodisperse systems. There are some small modifications to this procedure in the case of a binary system, which we will discuss in § 4. All quantities are defined in lattice-Boltzmann units, that is, length is in units of the nearest neighbour lattice distance δl, and time in units of simulation time step δt. Thus, all values listed below for diameters, velocities and viscosities are in units of δl, $\delta l/\delta t$ and $\delta l^2/\delta t$, respectively. For the monodisperse simulations, $N = 54$ particles with a diameter d (typically between 8 and 25 lattice spacings) are distributed randomly in a box of $n_x \times n_y \times n_z$ lattice sites, by means of a standard Monte Carlo procedure for hard spheres. The size of the box is chosen such that $\phi^{sim} = N\pi d^3/(6n_x n_y n_z)$ is as close as possible to the desired packing fraction ϕ, where the deviation with ϕ^{sim} is in any case smaller than 0.005. Subsequently, the result for the drag force is then extrapolated to exactly ϕ by a second-order Taylor expansion using the best theoretical estimate from § 2. Periodic boundary conditions are used. Note that d is slightly different from the diameter d_o that is used to set up the boundary nodes as described in the previous section. We will come back to this point in § 3.3. All spheres are set to move with the same constant velocity $\boldsymbol{v}^{sim}$ in an arbitrary direction, so that the array of spheres moves as a static configuration through the system. The force $\boldsymbol{F}_{g\rightarrow s,i}$ that the LB gas exerts on each particle i is recorded in time, but not actually applied to the particle, so that it keeps moving with the same velocity. It is therefore necessary to apply a uniform force to the gas, which balances the total force that the particles exert on the gas phase, so that the total net momentum of the system is zero. This force will thus induce a backflow velocity $\boldsymbol{u}$ for the gas phase, such that

$$\phi V \rho_s \boldsymbol{v}^{sim} + (1-\phi) V \rho \boldsymbol{u} = 0,$$

with ρ_s, ρ the density of the solid and gas phase, respectively; we set $\rho_s = \rho$, so that the backflow force gives the superficial velocity of the gas in a frame of reference where the particles are static as equal to

$$\boldsymbol{U} = (1-\phi)(\boldsymbol{u} - \boldsymbol{v}^{sim}) = -\boldsymbol{v}^{sim}.$$

Typically, after some 50 000 time steps, a steady state is obtained where the average force on a particle $\sum_i \boldsymbol{F}_{g\rightarrow s,i}/N$ is found to fluctuate around a plateau value $\bar{\boldsymbol{F}}_{g\rightarrow s}$. The normalized drag force as defined in § 2 is then obtained by (see (5) and (6)):

$$F = \frac{(1-\phi)\bar{\boldsymbol{F}}_{g\rightarrow s}}{-3\pi\mu d \boldsymbol{v}^{sim}}. \tag{30}$$

In almost all simulations, the kinematic viscosity $\nu = \mu/\rho$ is set to $\nu = 0.0008333$. The final estimate for the drag force and its standard deviation, is obtained from the average over 10–30 independent simulations, where we varied both the configuration and the direction of the particle velocity; for the bidisperse simulations, we averaged over 5–10 independent configurations. In all cases, the magnitude of the velocity was such that the particle Reynolds number was smaller then 0.2; a few simulations have been performed with $Re = 1$. We found that extrapolation of the drag force to $Re^2 = 0$ was indistinguishable from the $Re = 0.2$ result, with respect to the error margin in the data. Therefore, the simulations are performed under effectively zero-Reynolds-number conditions.

The traditional method of obtaining the drag force in these types of simulation is by inducing a gas flow via a pressure gradient, whilst keeping the solid particles

https://doi.org/10.1017/S0022112004003295 Published online by Cambridge University Press

fixed to their positions. Such a pressure gradient can be generated either by applying the appropriate boundary conditions or by applying a uniform body force. The drawback of this method is that, apart from the drag force, the gas velocity also has to be measured, which introduces additional fluctuations in the final estimate. By contrast, in expression (30), all quantities except $\bar{\boldsymbol{F}}_{g\to s}$ are set in the simulations. A second advantage is that if the particles move on the lattice, the boundary node configuration is fluctuating rather than static, which will diminish the artefacts due to the surface discretization, in particular since the effective diameter (see next section) is also obtained for a non-static boundary node configuration.

3.3. *Finite size effects*

As with any method that uses discretization, the effect of the grid size on the final result should be investigated. One effect of the lattice is that the actual diameter of the spheres is not *a priori* known, since the surface is represented by a set of lattice sites closest to some target diameter d_o, which is not necessarily equal to the true hydrodynamic diameter d. As suggested by Ladd (1993*a*, *b*), can obtain an estimate for d by a calibration experiment which involves measuring the drag force on a single sphere (with boundary nodes set by d_0), in a dilute system with periodic boundary conditions, by the method described in the previous section. The theoretical expression for the drag force on a sphere in a dilute cubic array is given by Hashimoto (1959):

$$\boldsymbol{F}_d = 3\pi\mu d\boldsymbol{U}(1-\phi)\left[1-1.7601\phi^{1/3}+\phi-1.5593\phi^2+O(\phi^3)\right]^{-1},$$

from which the diameter d can then be obtained. In general, it is found that d is larger than d_o, depending on the viscosity. Values for d are provided with the SUSP3D code up to $d_o = 16.4$. We have performed the calibration also for $d_o = 24.4$ and $d_o = 32.4$, with the kinematic viscosity equal to 0.0008333. A best fit in the range $4 < d_o < 33$ is given by

$$\frac{d}{d_o} = 1 + \frac{1}{1.17 + 0.85 d_o}.$$

Note that this calibration is performed for low volume fractions, and therefore only concerns the direct linear dependence of the drag force on d; in other words, it ensures that the correct value for d is used in the factor $3\pi\mu d\boldsymbol{U}$ by which the measured drag force is normalized. However, the drag force also depends indirectly on the diameter, since d sets the volume fraction; from the Carman–Kozeny relations, it follows that for dense systems (say around $\phi = 0.5$) an increase of 1% in d will result in an increase of almost 10% in F. A related problem for dense systems is that with relatively small particle diameters there will be insufficient lattice points in the gaps between the spheres to accurately describe the gas flow. A reasonable estimate for the average pore diameter is given by the hydraulic radius $r_h = d(1-\phi)/6\phi$; note that this implies that, for example, at packing $\phi = 0.5$, a diameter of $d = 6$ will lead to, on average, a single lattice point between the spheres. For these reasons, we have performed simulations with diameters $d_o = 9.6$, 12.4, 16.4 and 24.4, for packing fractions 0.5 and 0.7. As shown in figure 2 (for $\phi = 0.5$) and figure 3 (for $\phi = 0.7$), the drag force is clearly dependent on the average number of grid points in the pore, and found to scale roughly as $1/r_h^2$. In figures 2 and 3, the solid squares represent our lattice-Boltzmann data for a viscosity $\nu = 0.0008333$; The star represents the data from Hill *et al.* (2001*a*, *b*). From figures 2 and 3, it follows that the values for F obtained with the

https://doi.org/10.1017/S0022112004003295 Published online by Cambridge University Press

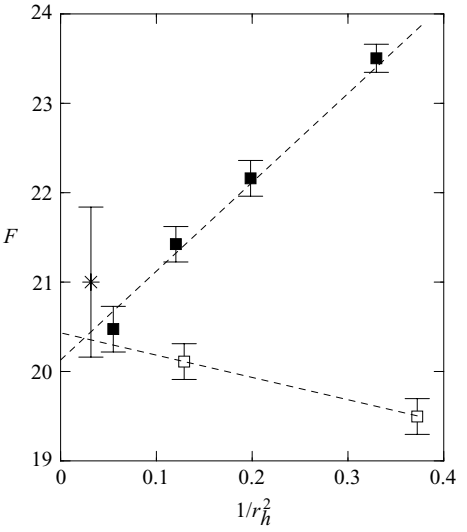

FIGURE 2. Normalized drag force as a function of $1/r_h^2$, where r_h is roughly equal to the number of grid points in between the spheres. The solid and open squares are for viscosities $\nu = 0.0008333$ and $\nu = 0.1667$, respectively. The star represents the lattice-Boltzmann data of Hill *et al.* (2001*a*, *b*). The intersection of the dashed line with the y-axis represents the best estimate for the drag force. The packing fraction for this system was equal to $\phi = 0.5$.

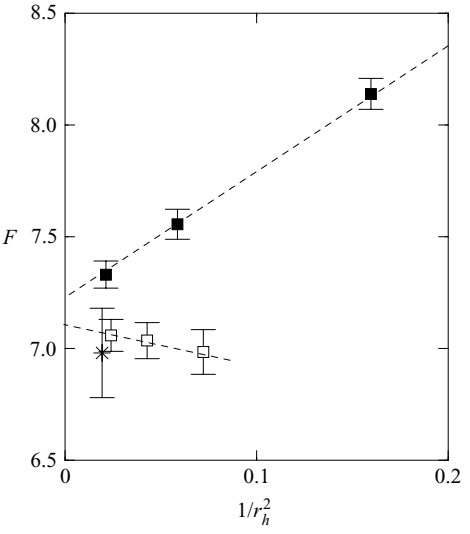

FIGURE 3. As figure 2, but for packing fraction $\phi = 0.3$.

largest diameters ($d_o = 24.4$ and 16.2 for $\phi = 0.5$ and 0.3, respectively), corresponding to about 5 grid points per pore, still have a small but significant deviation from the extrapolated value at $r_h = \infty$. Therefore, for each packing fraction we have performed simulations for two different values of r_h, where the final value for the drag force is obtained from the linear extrapolation of F *vs.* r_h^{-2} to $r_h^{-2} = 0$. In the lattice-Boltzmann simulations reported by Hill *et al.* (2001*a*, *b*), r_h is typically around 4 to 5 grid points for the dense systems.

https://doi.org/10.1017/S0022112004003295 Published online by Cambridge University Press

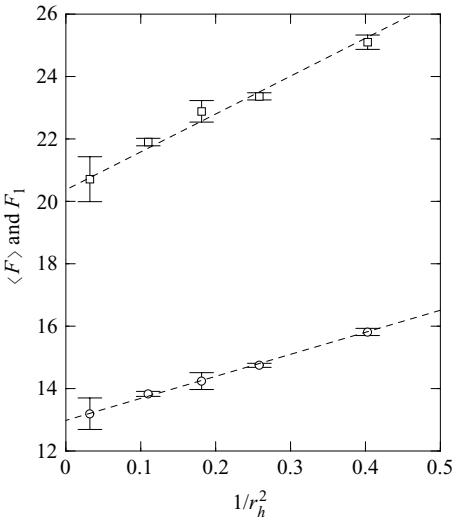

FIGURE 4. Simulation results for the drag force in a binary system as a function of $1/r_h^2$. The squares represent the data for the average drag force (19); the circles represent the data for the individual drag force F_1 on the particles with diameter d_1. Overall packing fraction, viscosity and diameter ratio are equal to $\phi = 0.5$, $\nu = 0.0008333$, and $d_1/d_2 = 0.5$, respectively.

In principle, the normalized drag force should not depend on the viscosity of the gas. In figures 2 and 3, the open squares represent the result from simulations with a viscosity that is 200 times larger ($\nu = 0.1667$), where we also increased the velocity of the particles by a factor of 200, to a value of 0.001, so that the Reynolds number is not changed. Note that this value for the velocity is still sufficiently small compared to the speed of sound $c_s = \sqrt{0.5}$. There are significant deviations between the two sets of results, however, the values extrapolated to $r_h = \infty$ are in good agreement. We have performed all simulations reported in §§4 and 5 with the smallest viscosity.

For binary systems, the finite size effects are similar to those in monodisperse systems. In figure 4, we show both the normalized drag force F_1 on particles of type 1, and the average drag force $\langle F \rangle$ defined by (19), for a system with $d_1/d_2 = 0.5$, equal mass fractions, and an overall packing fraction $\phi = 0.5$. Again, we find that the drag force scales as $1/r_h^2$; therefore also in our binary simulations, we have collected data for two different sets of particle diameters, were the final value is the linear extrapolation of F to $r_h^{-2} = 0$.

4. Simulation results

4.1. *Monodisperse systems*

In table 1, we give the results from our lattice-Boltzmann simulations for the drag force in a random array of monodisperse spheres, measured via the procedure outlined in § 3. In table 1, k_{sim} represents the Kozeny constant that would correspond to the measured drag force, i.e. $k_{sim} = F(1-\phi)^2/(2\phi)$. We find that for dense systems, its value is very close to the experimental value of 5. In figure 5, we compare our simulation results (square symbols) with two other sets of numerical data from literature. In figure 5, the triangles represent the data of Ladd (1990), obtained via a multipole expansion of the force density on the surface of the spheres, where the fluid motion is described by the Stokes equations. The circles represent the lattice-Boltzmann data

https://doi.org/10.1017/S0022112004003295 Published online by Cambridge University Press

ϕ	F	ΔF	k_{sim}
0.10	2.44	0.04	9.90
0.20	4.25	0.07	6.80
0.30	7.22	0.06	5.90
0.35	8.90	0.14	5.37
0.40	11.97	0.12	5.39
0.45	15.45	0.13	5.19
0.50	20.10	0.22	5.03
0.55	27.40	0.24	5.04
0.60	38.85	0.33	5.18

TABLE 1. Results from the lattice-Boltzmann simulations for the normalized drag force F in monodisperse arrays of spheres at packing fraction ϕ; ΔF is an estimate for the error in F, and k_{sim} is the Kozeny constant as calculated from the simulation data.

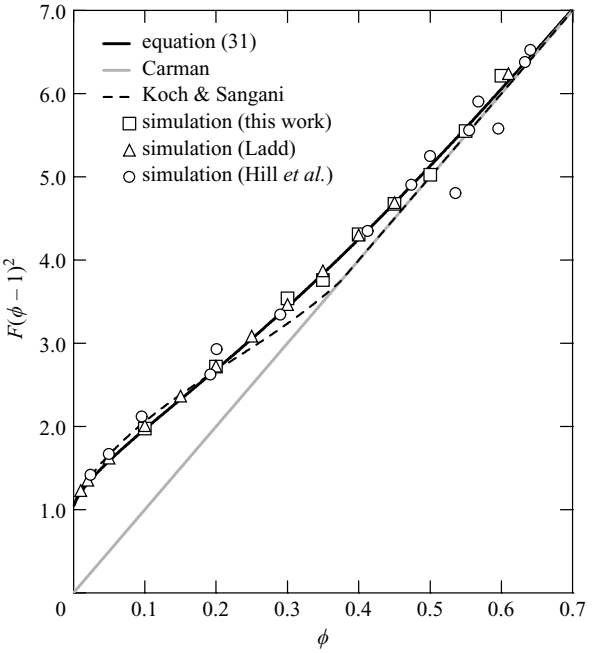

FIGURE 5. Normalized drag force (multiplied by the porosity squared) as a function of the packing fraction ϕ. The symbols represent the simulation data, from this work (squares), Ladd (1990) (triangles), and Hill *et al.* (2001*a*, *b*)(circles). The triangle symbol at $\phi = 0.61$ represents data taken from Kang & Sangani (1994). The black line represents the best fit (31) to all simulation data. Also shown are the correlations by Carman (grey line) and Koch & Sangani (dashed line).

of Hill *et al.* (2001*a*, *b*). We find that our data are in very good agreement with Ladd's results, and consistent with the results of Hill *et al.* (2001*a*, *b*). Note that the latter data suffer from somewhat more scattering, in particular for higher packing fractions, which could be caused by insufficient sampling. In our simulations, we found that for densely packed systems, the individual results for each configuration can be very different, owing to the limited number of particles. Rather than increasing the number of particles, we decided to obtain data for more independent configurations and flow

https://doi.org/10.1017/S0022112004003295 Published online by Cambridge University Press

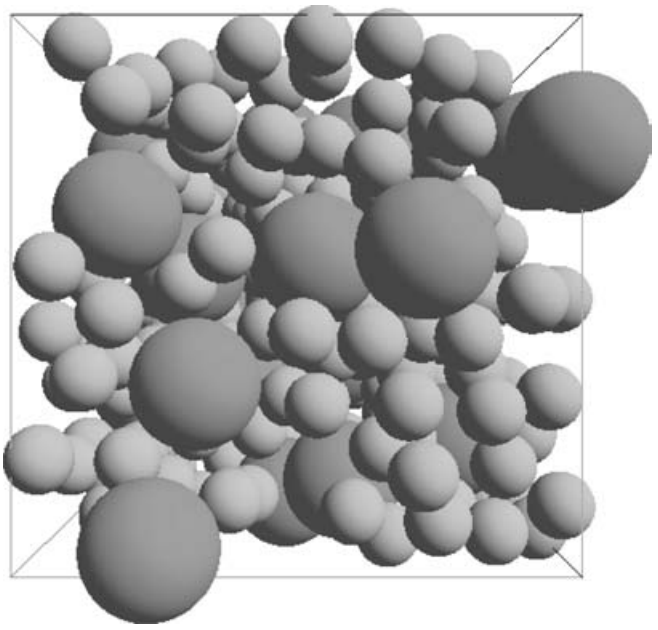

FIGURE 6. Example of a binary configuration of 24 large spheres and 192 small spheres; for this system $\phi = 0.5$, $d_2/d_1 = 0.5$ and $\phi_1/\phi_2 = 1$. Note that in the simulations, periodic boundary conditions are employed in all directions.

directions (30 in total), and in the final average omitted all data that were outside 2.5 times the standard deviation, as calculated from the initial average. The solid line in figure 5 is our best fit to all simulation data, which takes the following simple form:

$$F(\phi) = 10\frac{\phi}{(1-\phi)^2} + (1-\phi)^2(1+1.5\sqrt{\phi}), \tag{31}$$

i.e. the Carman equation with a term added in order to have the correct limiting behaviour for $\phi \to 0$. The largest deviation of this fit with either the present lattice-Boltzmann data and Ladd's multipole expansion data is 3%; about the same margin of error is found with the multipole expansion data by Mo & Sangani 1994. Since all these data sets are obtained by two completely independent simulation methods, we claim that (31) represents the true drag force for random arrays of monodisperse spheres to within 3%, and probably less. For comparison, in figure 5 we also show the Carman equation (grey line), and the fit (14) proposed by Koch & Sangani (1999) (dashed line). For a comparison with the other predictions from § 2.2, we refer to figure 1, which is drawn on the same scale as figure 5.

4.2. *Bidisperse systems*

In the bidisperse simulations, the total number of particles ranged from 64 to 1000, depending on the composition and diameter ratio. A typical example of a configuration, obtained via a standard Monte Carlo procedure for binary hard spheres, is shown in figure 6. A particular problem with the large diameter ratios that we studied (up to 1:4) was that the number of large spheres becomes very low. The system sizes that we studied were, in any case, such that there are at least 12 large particles present. In table 2, we show the final results for the normalized drag force (16) for a range of packing fractions, diameter ratios and mass fractions. The

https://doi.org/10.1017/S0022112004003295 Published online by Cambridge University Press

ϕ	$\frac{d_1}{d_2}$	ϕ_1	F_1	F_2	$\frac{\langle F\rangle}{F}$	k_{sim}
0.10	0.500	0.050	2.11	3.63	1.11	10.9
0.10	0.700	0.051	2.16	2.90	1.02	10.0
0.25	0.500	0.188	4.81	12.05	1.05	6.4
0.25	0.500	0.124	3.98	9.29	1.03	6.3
0.25	0.500	0.062	3.33	7.09	1.02	6.2
0.25	0.607	0.188	4.88	9.18	1.02	6.2
0.25	0.607	0.123	4.43	8.37	1.08	6.6
0.25	0.607	0.062	3.60	6.53	1.00	6.1
0.25	0.607	0.046	3.64	6.40	1.04	6.3
0.25	0.700	0.187	5.03	7.81	1.02	6.2
0.25	0.700	0.127	4.49	7.04	1.01	6.2
0.25	0.700	0.064	4.19	6.14	1.01	6.2
0.35	0.500	0.174	6.31	17.02	1.04	5.7
0.35	0.700	0.178	7.54	12.24	1.03	5.6
0.40	0.250	0.203	7.23	62.34	1.19	6.3
0.40	0.250	0.101	4.67	33.72	1.21	6.4
0.40	0.333	0.301	9.29	55.96	1.04	5.5
0.40	0.333	0.202	6.98	37.69	1.06	5.6
0.40	0.333	0.100	5.14	25.26	1.15	6.1
0.40	0.500	0.300	9.86	29.34	1.02	5.4
0.40	0.500	0.199	8.15	23.33	1.05	5.6
0.40	0.500	0.099	6.47	16.57	1.03	5.5
0.40	0.607	0.300	9.84	21.54	0.97	5.2
0.40	0.607	0.197	8.78	18.14	1.02	5.4
0.40	0.607	0.073	6.80	13.33	0.97	5.1
0.40	0.700	0.299	10.20	17.41	0.97	5.2
0.40	0.700	0.203	9.05	15.08	0.96	5.1
0.40	0.700	0.102	8.38	13.62	1.00	5.3
0.50	0.250	0.253	10.71	112.51	1.09	5.6
0.50	0.250	0.126	6.65	59.27	1.12	5.8
0.50	0.333	0.377	15.71	106.63	1.03	5.3
0.50	0.333	0.253	11.44	74.57	1.07	5.5
0.50	0.333	0.125	7.38	43.09	1.06	5.4
0.50	0.500	0.450	18.67	61.84	0.99	5.1
0.50	0.500	0.375	17.37	56.40	1.05	5.4
0.50	0.500	0.250	12.98	40.47	1.00	5.1
0.50	0.500	0.125	10.27	31.05	1.05	5.4
0.50	0.500	0.050	8.46	24.52	1.03	5.3
0.50	0.500	0.025	7.23	21.24	0.96	4.9
0.50	0.607	0.375	17.60	40.92	1.02	5.2
0.50	0.607	0.249	14.26	32.48	0.99	5.1
0.50	0.607	0.123	11.65	25.34	0.97	5.0
0.50	0.607	0.092	10.95	24.59	0.99	5.1
0.50	0.700	0.374	18.20	33.24	1.01	5.2
0.50	0.700	0.254	15.44	27.46	0.97	5.0
0.50	0.700	0.128	12.93	24.41	0.99	5.1
0.60	0.500	0.300	23.04	76.87	0.99	5.0
0.60	0.607	0.110	19.49	44.95	0.98	4.9
0.60	0.700	0.304	27.93	50.81	0.96	4.9

TABLE 2. Results from the lattice-Boltzmann simulations for the normalized drag force F_1 and F_2 in a bidisperse arrays of spheres; the system parameters that have been varied are the packing fraction ϕ, the diameter ratio d_1/d_2 and the volume fraction ϕ_1 of the small spheres. $\langle F\rangle/F$ is the average drag force (see (19)) divided by the monodisperse drag force at the same ϕ, and k_{sim} the Kozeny constant as calculated from the average drag force.

subscripts '1' and '2' refer to the small and the large spheres, respectively. In the last two columns, we show the average properties as calculated from the data in the first five columns. In table 2, $\langle F\rangle/F$ is the average drag force (19), divided by the best fit to the monodisperse drag force at the same ϕ, given by (31). It shows that our central assumption (21), that is, the average drag force equals the monodisperse drag force at the same ϕ, is indeed reasonably valid; in fact, if we disregard the data for the most extreme diameter ratio (1:4), the agreement is within about 10%, and in most cases of the order of 5%. The fact that the systems with large diameter ratios conform less well to the assumption (21), which was based on the Carman–Kozeny analysis, could have several reasons. First, the number of large spheres in these systems it very small, so the measured drag force is expected to depend very much on the actual configuration, where we averaged over only five different configuration. A second reason could be that the Carman–Kozeny analysis is not valid for large diameter ratios. Indeed, table 2 seems to indicate that the average drag force for large

https://doi.org/10.1017/S0022112004003295 Published online by Cambridge University Press

diameter ratios is systematically larger than the monodisperse drag force. Clearly, more accurate simulations (larger systems and more configurations) are desirable, but at present prohibitively expensive.

The last column in table 2 is shown in order to make contact with the experimental results for the resistance behaviour of binary systems from the literature, which are mainly presented in terms of a permeability and the corresponding Kozeny constant. In table 2, k_{sim} represents the Kozeny constant derived from the simulation data under the assumption that the Carman–Kozeny relation is strictly valid, i.e. $k_{sim} = \langle F \rangle (1-\phi)^2/(2\phi)$. We find that on approaching closed packing, k_{sim} tends to settle at a value of 5, which was also found in the monodisperse systems; of course, this observation is completely consistent with the fact that $\langle F \rangle / F$ approaches 1. We found an average value $k = 5.36$ for the data in the range $0.30 < \phi < 0.60$, which is in extremely good agreement with the experimental result $k = 5.34$ by Fand *et al.* (1987). It is also consistent with the experimental results by Coulson, as reported in the original paper by Carman (1937). For bidisperse mixtures, Coulson found Kozeny constants in the range 5.0–5.9. Thies-Weesie & Philipse (1994) studied the flow of cyclohexane through silica sphere packings for several sphere size and mixture compositions. They found that the Carman–Kozeny type scaling was valid, but report a much lower value for the Kozeny constant: $k = 4.0$. Maier *et al.* (1999) used the lattice-Boltzmann method to simulate systems comparable to those of Thies-Weesie & Philipse, and report slightly higher values for the Kozeny constant $k = 4.7$–5.3. Two possible explanations for the difference with the Thies-Weesie & Philipse data were given: the porosity in the experiments may have decreased during sintering after the measurement, or there could have been some local ordering near the walls.

The final conclusion on the basis of our data, and the experimental findings, is that if a Carman–Kozeny scaling for the permeability is assumed, the value for the Kozeny 'constant' will roughly increase from 5.0 to 6.0 on loosening the packing from $\phi = 0.5$ to 0.3. This implies that the scaling itself is not strictly valid, as was found in the monodisperse systems. Nevertheless, the Carman–Kozeny relation remains a very useful description for both mono- and bidisperse systems, when a value of $k = 5$ is adopted (i.e. the Carman equation), and subsequently a correction term for higher porosities is included, see (31).

Thus far, the discussion is concerned with the average drag force on the particles, which is sufficient to predict the permeability and thereby the pressure drop over the system, see (18). However, in the chemical engineering models of gas–solid flow, the individual drag force on the small and large particles is required. As discussed in § 2.3, at present the assumption is made that the non-normalized drag force $\boldsymbol{F}_{d,i}$ scales with d_i. This *ad hoc* assumption has not yet been tested, since no numerical and experimental data were available for individual drag force, apart from some very recent data by Koo & Sangani (2002). The approximation $\boldsymbol{F}_{d,i} \sim d_i$ implies that the ratio of the normalized drag force $F_2/F_1 = 1$, independent of the diameter ratio. In figure 7, we show F_2/F_1 *vs.* d_2/d_1, calculated from the simulation results of table 2. The figure indicates that $F_2/F_1 = (d_2/d_1)^n$, with n in between 1 and 2. On the basis of this, and from the fact that $\langle F \rangle \approx F(\phi)$, we propose the following expression for F_i (see § 2.4):

$$F_i(\phi, y_i) = \left((1-\phi)y_i + \phi\, y_i^2\right) F(\phi), \qquad y_i = \frac{d_i}{\langle d \rangle}, \tag{32}$$

with $F(\phi)$ given by (31). In figure 8, we plot our simulation data for F_i, normalized by $F(\phi)$, against $(1-\phi)y_i + \phi y_i^2$. The solid line represent F_i/F according to (32).

https://doi.org/10.1017/S0022112004003295 Published online by Cambridge University Press

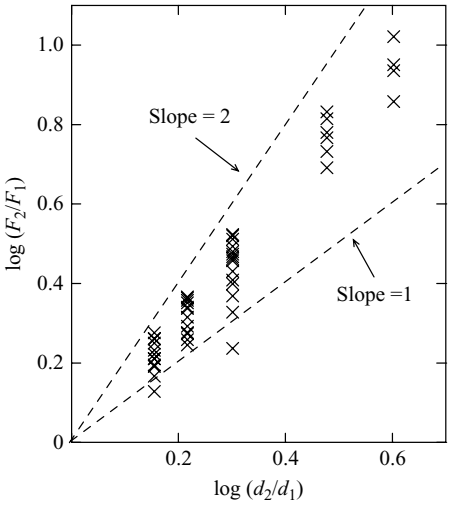

FIGURE 7. Log–log plot of the force ratio as function of the diameter ratio.

For the smaller spheres ($y_i < 1.4$), we find very good agreement, and some small but systematic deviations for the larger spheres, similar to what was observed for the average drag force. If the most extreme systems ($d_1/d_2 = 0.25$ and 0.33, and $\phi = 0.1$) are not taken into account, then the correlation (32) describes the data on average within 4%, with a maximum deviation of 14%, where we stress that this level of agreement is achieved without the use of any adjustable parameter. By including a single fit parameter, namely the coefficient of an additional term $(1-\phi)y_i^3$ in (32), a reasonable agreement with the data for all diameter ratios and packing fractions can be obtained:

$$F_i(\phi, y_i) = \left((1-\phi)y_i + \phi y_i^2 + 0.064(1-\phi)y_i^3\right) F(\phi). \tag{33}$$

Note that by including a term y_i^3, the average drag force $\langle F \rangle$ as calculated from F_i will no longer be equal to the monodisperse drag force F, but slightly larger for larger diameters, in accordance with the data in table 2. The maximum deviation of the data in table 2 with (33) is 16%, where the average deviation is 5% (see also figure 9). To our knowledge, the only accurate data in literature on the individual drag force is by Koo & Sangani (2002), who used a multipole expansion for two size ratios (0.5 and 0.7) and two packing fractions (0.1 and 0.35); their data, indicated by the plus symbols in figure 8, is in good agreement with our data, and (32).

Finally, we want to test how the predictions for the individual drag force from the Patwardhan & Tien (PT) model (see § 3.3) compare to the predictions from (33). In figure 9, we show the relative deviation of the simulation data for F_i with the various predictions; for details we refer to the figure caption. We find that (33) and the PT model with the exact δ describe the numerical data equally well, where the relative deviations seem to be opposite. It should be noted that in the original paper, Patwardhan & Tien propose to use a mean distance δ given by (24), which is found to give deviations of more than 100% (not shown in the figure).

5. Summary and conclusions

We want to summarize this work by restating the most important results, which is also useful for quick reference. For monodisperse systems in the limit of zero

https://doi.org/10.1017/S0022112004003295 Published online by Cambridge University Press

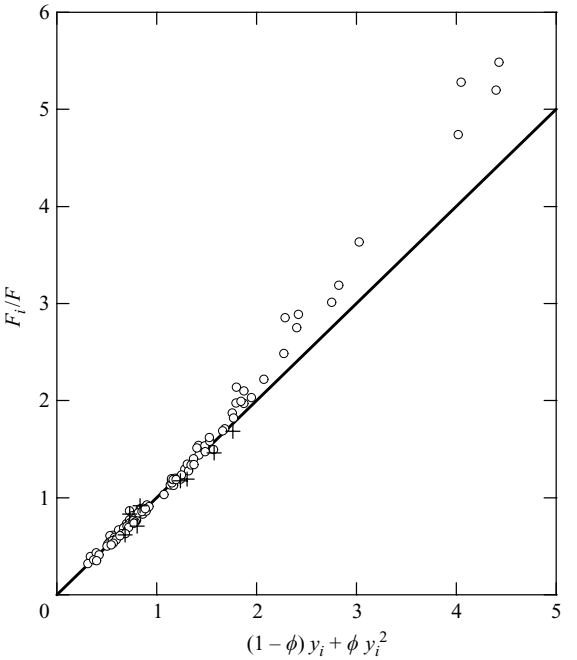

FIGURE 8. Individual drag force F_i divided by the drag force F of a monodisperse system at the same ϕ, as a function of $(1-\phi)y_i+\phi y_i^2$. The circles represent the simulation data from table 2, the plus symbols the simulation results from Koo & Sangani (2002); the solid line is the theoretical prediction given by (32). Note that assumption $F_i = F$, which is used in many numerical models, differs by up to a factor of 5 with the simulation data.

Reynolds number, we propose the following expression for normalized drag force F defined by (6):

$$F(\phi) = 10\frac{\phi}{(1-\phi)^2} + (1-\phi)^2(1+1.5\sqrt{\phi}), \tag{34}$$

which corresponds to a pressure drop per unit length:

$$\nabla P_{mono} = -\frac{\mu \boldsymbol{U}}{d^2}\left[180\frac{\phi^2}{(1-\phi)^3} + 18\phi(1-\phi)(1+1.5\sqrt{\phi})\right].$$

Equation (34) is found to be in excellent agreement (deviation smaller than 3%) with the simulation data of Ladd (1990), Mo & Sangani (1994), Kang & Sangani (1994) and this work, over the entire range of packing fractions.

For polydisperse systems, we propose the following expression for the normalized drag force F_i as defined by (16):

$$F_i(\phi, y_i) = \left((1-\phi)y_i + \phi y_i^2 + 0.064(1-\phi)y_i^3\right) F(\phi), \qquad y_i = \frac{d_i}{\langle d\rangle}, \tag{35}$$

with $F(\phi)$ given by (34) and $\langle d\rangle$ defined in (17). The individual drag force is thus equal to the monodisperse normalized drag force, multiplied by a correction term that is dependent only on the diameter fraction y_i and the packing fraction ϕ. The corresponding pressure drop per unit length is equal to

$$\nabla P_{poly} = \nabla P_{mono}\frac{d^2}{\langle d\rangle^2}\left(1 - 0.064(1-\phi)\sum_i x_i y_i\right). \tag{36}$$

https://doi.org/10.1017/S0022112004003295 Published online by Cambridge University Press

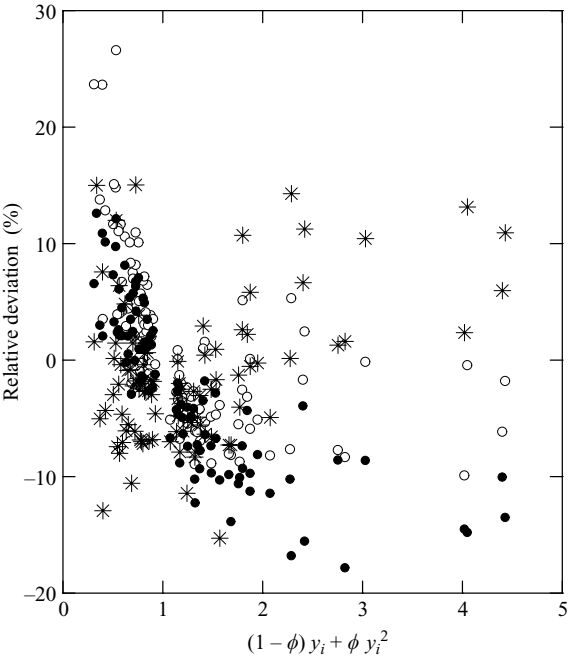

FIGURE 9. Relative deviation (percentage) of the simulation data for the individual drag force F_i. The circles represent the deviation with the PT model for $\delta = \langle d\rangle(\phi^{-1/3}-1)$ (open circles), and for the exact δ, solved from (25) (solid circles); the star symbols are the deviation of the simulation data with (33).

The average deviation of (35) with the simulation results in the range $0.1 \leqslant \phi \leqslant 0.6$ is less than 5%; by comparison, the assumption that $F_i = F$, which is primarily used for the numerical models of gas–solid flow, is out by a factor of 1.75 (on average) for diameter ratios 1:2, and a factor of 3.2 (on average) for diameter ratios 1:4. The only other model in the literature that includes a correction to the monodisperse drag force in the case of polydisperse particles is from Patwardhan & Tien. In its original form, deviations of more than 100% with the simulation data are found. An improvement is made when in the model d_{avg} is replaced by $\langle d\rangle$. As in (35), the correction can then be shown to depend only on the diameter fraction y_i

$$F_i(\phi, y_i) = F\left(\left(1+\frac{\phi^{-1/3}-1}{y_i}\right)^{-3}\right).$$

which was found to be accurate within 30%. However, the Patwardhan & Tien model can achieve the same level of accuracy as (35) by solving a cubic equation, involving higher-order moments of d_i. Clearly, for practical applications, (35) will be far more convenient to use.

We finally note that the expressions of § 2.4 are derived for a general polydisperse system, and we therefore expect (35) and (36) to be valid for those systems as well, although this should be tested in computer simulations; in the case where the polydisperse system is characterized by Gaussian-type size distribution of the diameters around $\bar{d}$, with a width σ, the average diameter $\langle d\rangle$ can be readily evaluated:

$$\langle d\rangle = \frac{3\sigma^2\bar{d}+\bar{d}^3}{\sigma^2+\bar{d}^2}. \tag{37}$$

https://doi.org/10.1017/S0022112004003295 Published online by Cambridge University Press

It has been argued that the discrepancy of the empirical Ergun equation (coefficient 150) with the numerical results (coefficient 180) can be attributed partly to the fact that the experimental systems were not strictly monodisperse. Inserting (37) into (36), and neglecting the term y_i^3 (which can be done safely if the diameter ratio is less than two) gives

$$\nabla P_{poly} = \nabla P_{mono} \left(\frac{(\sigma/d)^2 + 1}{3(\sigma/d)^2 + 1} \right)^2 .$$

It then follows that a polydispersity of about 22% (i.e. $\sigma/d = 0.22$), is sufficient to reduce the pressure gradient by $0.833 \approx 150/180$. However, other factors, such as inhomogeneity, might also play a role. This will be the subject of a future line of work, where we intend to move away gradually from the ideal situation of static homogeneous systems, towards the non-ideal situations as encountered in fluidized beds. Apart from inhomogeneity, the role of granular temperature will also be studied in detail.

We would like to thank Anthony Ladd for many useful discussions, and for allowing us to use his lattice-Boltzmann suspension code SUSP3D. This work is part of the research program of the 'Stichting voor Fundamenteel Onderzoek der Materie (FOM)', which is financially supported by the 'Nederlandse Organisatie voor Wetenschappelijk Onderzoek (NWO)'.

REFERENCES

Bokkers, G. A., van Sint Annaland, M. & Kuipers, J. A. M. 2004 Mixing and segregation in a bidisperse gas–solid fluidised bed: a numerical and experimental study. *Powder Technol.* in press.

Carman, P. C. 1937 Fluid flow through granular beds. *Trans. Inst. Chem. Engng* **15**, 150.

Chen, S. & Doolen, G. D. 1998 Lattice-Boltzmann method for fluid flow. *Annu. Rev. Fluid Mech.* **30**, 329.

Di Felice, R. 1995 Hydrodynamics of liquid fluidisation. *Chem. Engng Sci.* **50**, 1213.

Ergun, S. 1952 Fluid flow through packed columns. *Chem. Engng Proc.* **48**, 89.

Fand, R. M., Kim, B. Y. K., Lam, A. C. C. & Pan, R. T. 1987 Resistance of the flow of fluids through simple and complex porous media whose matrices are composed of randomly packed spheres. *Trans. ASME I: J. Fluids Engng* **109**, 268.

Gidaspow, D. 1994 *Multiphase Flow and Fluidization: Continuum and Kinetic Theory Descriptions.* Academic.

Hashimoto, H. 1959 On the periodic fundamental solutions of the Stokes equation and their application to viscous flow past a cubic array of spheres. *J. Fluid Mech.* **5**, 317.

Hill, R. J., Koch, D. L. & Ladd, A. J. C. 2001*a* The first effects of fluid inertia on flows in ordered and random arrays of spheres. *J. Fluid Mech.* **448**, 213.

Hill, R. J., Koch, D. L. & Ladd, A. J. C. 2001*b* Moderate-Reynolds-number flows in ordered and random arrays of spheres. *J. Fluid Mech.* **448**, 243.

Hoomans, B. P. B., Kuipers, J. A. M., Briels, W. J. & van Swaaij, W. P. M. 1996 Discrete particle simulation of bubble and slug formation in a two-dimensional gas-fluidized bed: a hard sphere approach. *Chem. Engng Sci.* **51**, 99.

Kang, S.-Y. & Sangani, A. S. 1994 Electrokinetic properties of suspensions of colloidal particles with thin, polarized double layers. *J. Colloid Interface Sci.* **165**, 195.

Kim, S. & Russel, W. B. 1985 Modeling of porous media by renormalization of the Stokes equation. *J. Fluid Mech.* **154**, 269.

Koch, D. L. & Hill, R. J. 2001 Inertial effects in suspension and porous media flow. *Annu. Rev. Fluid Mech.* **33**, 619.

Koch, D. L. & Sangani, A. S. 1999 Particle pressure and marginal stability limits for homogeneous monodisperse gas fluidized bed: kinetic theory and numerical simulations. *J. Fluid Mech.* **400**, 229.

https://doi.org/10.1017/S0022112004003295 Published online by Cambridge University Press

Koo, S. & Sangani, A. S. 2002 Effective-medium theories for predicting hydrodynamic transport properties of bidisperse suspensions. *Phys. Fluids* **14**, 3522.

Kuipers, J. A. M. & van Swaaij, W. P. M. 1998 Computational fluid dynamics applied to chemical reaction engineering. *Adv. Chem. Engng* **24**, 227.

Ladd, A. J. C. 1990 Hydrodynamic transport coefficients of random dispersions of hard spheres. *J. Chem. Phys.* **93**, 3484.

Ladd, A. J. C. 1993*a* Numerical simulations of particulate suspensions via a discretized Boltzmann equation. Part 1. Theoretical Foundation. *J. Fluid Mech.* **271**, 285.

Ladd, A. J. C. 1993*b* Numerical simulations of particulate suspensions via a discretized Boltzmann equation. Part 2. Numerical results. *J. Fluid Mech.* **271**, 311.

Ladd, A. J. C. & Verberg, R. 2001 Lattice-Boltzmann simulations of particle fluid suspensions. *J. Stat. Phys.* **104**, 1191.

Li, J. & Kuipers, J. A. M. 2003 Gas–particle interactions in dense gas-fluidized beds. *Chem. Engng Sci.* **58**, 711.

Maier, R. S., Kroll, D. M., Davis, H. T. & Bernard, R. S. 1999 Simulation of flow in bidisperse spheres packings. *J. Colloid Interface Sci.* **217**, 341.

Mo, G. & Sangani, A. S. 1994 A method for computing Stokes flow interactions among spherical objects and its application to suspensions of drops and porous particles. *Phys. Fluids* **6**, 1637.

Patwardhan, V. S. & Tien, C. 1985 Sedimentation and liquid fluidization of solid particles of different sizes and density. *Chem. Engng Sci.* **40**, 1051.

Sangani, A. S. & Yao, C. 1988 Bulk thermal-conductivity of composites with spherical inclusions. *J. Appl. Phys.* **63**, 1334.

Schiller, L. & Nauman, A. 1935 A drag coefficient correlation. *V.D.I. Zeitung* **77**, 318.

Succi, S. 2001 *The Lattice-Boltzmann Equation for Fluid Dynamics and Beyond*. Clarendon.

van Swaaij, W. P. M. 1985 Chemical Reactors. In *Fluidization* (ed. J. F. Davidson & R. Clift). Academic.

Thies-Weesie, D. M. E. & Philipse, A. P. 1994 Liquid permeation of bidisperse colloidal hard-sphere packings and the Kozeny relation. *J. Colloid Interface Sci.* **162**, 470.

Wen, C. Y. & Yu, Y. H. 1966 Mechanics of fluidization. *AIChE J.* **62**, 100.

https://doi.org/10.1017/S0022112004003295 Published online by Cambridge University Press